Ultrasonics 54 (2014) 2151–2158

Contents lists available at ScienceDirect

Ultrasonics

journal homepage: www.elsevier.com/locate/ultras

Periodic shock-emission from acoustically driven cavitation clouds: A source of the subharmonic signal

Keith Johnston [a], Cecilia Tapia-Siles [a], Bjoern Gerold [a,b], Michiel Postema [c], Sandy Cochran [a], Alfred Cuschieri [a], Paul Prentice [a,b,*]

[a] Institute for Medical Science and Technology, Division of Imaging and Technology, University of Dundee, Dundee DD2 1FD, UK
[b] Diagnostic Sonar Ltd., Livingston EH54 7BX, UK
[c] Department of Physics and Technology, University of Bergen, Allégaten 55, 5007 Bergen, Norway

ARTICLE INFO

Article history:
Received 5 March 2014
Received in revised form 9 June 2014
Accepted 9 June 2014
Available online 27 June 2014

Keywords:
Acoustic cavitation
Subharmonic
Cloud dynamics
Collapse
Shock-wave

ABSTRACT

Single clouds of cavitation bubbles, driven by 254 kHz focused ultrasound at pressure amplitudes in the range of 0.48–1.22 MPa, have been observed via high-speed shadowgraphic imaging at 1×10^6 frames per second. Clouds underwent repetitive growth, oscillation and collapse (GOC) cycles, with shock-waves emitted periodically at the instant of collapse during each cycle. The frequency of cloud collapse, and coincident shock-emission, was primarily dependent on the intensity of the focused ultrasound driving the activity. The lowest peak-to-peak pressure amplitude of 0.48 MPa generated shock-waves with an average period of 7.9 ± 0.5 μs, corresponding to a frequency of $f_0/2$, half-harmonic to the fundamental driving. Increasing the intensity gave rise to GOC cycles and shock-emission periods of 11.8 ± 0.3, 15.8 ± 0.3, 19.8 ± 0.2 μs, at pressure amplitudes of 0.64, 0.92 and 1.22 MPa, corresponding to the higher-order subharmonics of $f_0/3$, $f_0/4$ and $f_0/5$, respectively. Parallel passive acoustic detection, filtered for the fundamental driving, revealed features that correlated temporally to the shock-emissions observed via high-speed imaging, p(two-tailed) < 0.01 (r = 0.996, taken over all data). Subtracting the isolated acoustic shock profiles from the raw signal collected from the detector, demonstrated the removal of subharmonic spectral peaks, in the frequency domain. The larger cavitation clouds (>200 μm diameter, at maximum inflation), that developed under insonations of peak-to-peak pressure amplitudes >1.0 MPa, emitted shock-waves with two or more fronts suggesting non-uniform collapse of the cloud. The observations indicate that periodic shock-emissions from acoustically driven cavitation clouds provide a source for the cavitation subharmonic signal, and that shock structure may be used to study intra-cloud dynamics at sub-microsecond timescales.

1. Introduction

Acoustic cavitation refers to the presence of bubbles in a liquid host medium on exposure to acoustic radiation. Applications that involve cavitation in moderate to high intensity insonations include sonochemistry [1], acoustic cleaning [2] and a relatively new field of medical therapy [3–5]. For the latter, cavitation in high intensity focused ultrasound (HIFU) is being investigated for its potential to selectively permeabilise regions of tissue, for the purpose of targeted drug delivery [6,7]. An improved understanding of acoustically driven cavitation dynamics, and particularly the detection and interpretation of signals emitted by bubble activity, are crucial for further development and refinement of such applications.

Cavitating bubbles act as secondary acoustic sources, and the spectrum of the signal generated is known to be strongly dependent on the frequency and intensity of the primary insonation, as well as characteristics of the bubble population itself [8–10]. Broadly, for a given driving frequency f_0, cavitation can be classified as stable at low intensities and non-stable, or inertial, at higher intensities. At very low intensities, linear bubble response produces emitted signal at f_0. Increasing the intensity, but remaining within the stable regime, will cause bubbles to oscillate non-linearly, which generates harmonics of the fundamental (nf_0), and weak, often intermittent subharmonic signal ($f_0/2$) and ultra-subharmonics ($(2n+1)f_0/2$). Above a threshold intensity, inertial cavitation is associated with a marked and sudden increase in broadband white noise, although strong harmonics and

* Corresponding author at: Institute for Medical Science and Technology, Division of Imaging and Technology, University of Dundee, Dundee DD2 1FD, UK.
E-mail address: p.prentice@dundee.ac.uk (P. Prentice).

http://dx.doi.org/10.1016/j.ultras.2014.06.011
0041-624X/

subharmonics persist. In addition, higher-order subharmonics (nf_0/m, $m > n$) become apparent on increasing the intensity through the threshold value, along with a corresponding set of ultra-subharmonics, above the fundamental [11].

A number of mechanistic sources for the subharmonic (and ultra-subharmonic) signals have been suggested theoretically and somewhat corroborated experimentally, although the topic remains the source of ongoing debate. In particular, larger bubbles within a population, having grown beyond the resonant size via rectified diffusion [12] or coalescence [13] for example, are known to be capable of oscillating at $f_0/2$ [14]. However, this is considered to be a less likely explanation for the higher-order subharmonics, owing to instabilities disrupting a bubble of the required size [15]. Furthermore, the subharmonic is detected from cavitation occurring in standing-wave fields [16], where larger than resonant bubbles are expected to be forced away from the pressure antinodes, and so this does not provide a wholly satisfactory explanation [15]. The occurrence of surface waves along the cavity interface could also provide a source [17], but is considered to be a weak contribution at best [18]. Chaotic bubble oscillations, which generate $f_0/2$ via period-doubling, and higher-order subharmonics through successive bifurcations, have also received a significant level of theoretical attention [19–21]. It is notable that single bubble mechanisms have predominantly been considered.

Nonetheless, acoustic detection at $f_0/2$ is commonly used to determine the onset of cavitation in the applications mentioned, particularly medical therapy, where it has been correlated to a range of associated bioeffects including enhanced heating [3], mechanical tissue damage [4] blood brain barrier disruption [5], and blood-clot dissolution [22]. The $f_0/2$ subharmonic is a convenient detection frequency, as the driving intensities typically employed will produce cavitation in the regime where subharmonic emissions are prominent. Moreover, higher harmonics of f_0 can occur in the absence of any cavitation activity, due to non-linear propagation of a sufficiently intense acoustic wave itself [23], and thus are not attractive detection frequency options.

In this paper, we employed the laser-nucleation technique [24,25] to observe cavitation clouds evolving from the instant of formation, through the first ~50 cycles of a 254 kHz focused ultrasound exposure. The novel experimental architecture used ensures cloud response to a purely propagating and well characterised focused ultrasound exposure, without reflection or scatter, was investigated. Ultra-high speed shadowgraphic photography over the duration of the HIFU exposure, facilitated observation of the emission of periodic shock-waves, coincident to strong concerted collapses of the driven cloud. In parallel, acoustic signals, which included subharmonic and higher-order subharmonic content, were collected via a passive cavitation detector (PCD) and directly correlated to the high-speed observations.

2. Experimental setup

2.1. The HIFU source

A HIFU transducer was fabricated, in-house, from a 63.2 mm diameter spherically focused, thereby defining the focal distance, single element PZ 26 piezoceramic (Meggit-Ferroperm, Kvistgard, Denmark). Impedance analysis (4395A, Agilent Technologies, CA, USA) revealed a fundamental resonance at $f_0 = 254$ kHz, and a lateral mode at 36 kHz. The device was driven with a sinusoidal signal from a waveform generator (DG4102, Rigol Technologies, Beijing, China) passed through an RF power amplifier (2100L, Electronics and Innovation, NY, USA). The peak-to-peak pressure amplitude (PA_{pp}) values used during the experiments were measured via the radiation force balance approach (RFB, Precision Acoustics, Dorchester, UK). A 254 kHz fundamental frequency was selected, primarily to ensure good temporal resolution of the cavitation dynamics, which were to be imaged at 1×10^6 frames per second (Mfps). We also note that this frequency of operation is close to that employed by the latest ExAblate® Neuro transducer (InSightec Ltd., Haifa, Israel) for focused ultrasound surgery of the brain at 220 kHz, under magnetic resonance imaging (MRI)-guidance.

2.2. The sonoptic chamber and high-speed imaging

A 'sonoptic' chamber was designed and constructed via rapid prototyping (uPrint SE, Stratasys, MN, USA), to conduct cavitation studies in the focused ultrasound field generated by the transducer described. A full description of the sonoptic chamber concept, its key features and the regimes of acoustic-laser cavitation that can be studied with such a set-up, is available, Gerold et al. [24]. Briefly, a distinctive 'square hour-glass' architecture, accommodates the field of the transducer which was fixed horizontally on the base ($150 \times 150\ mm^2$), to generate HIFU that propagates upwards through the chamber, without reflection of scatter. This

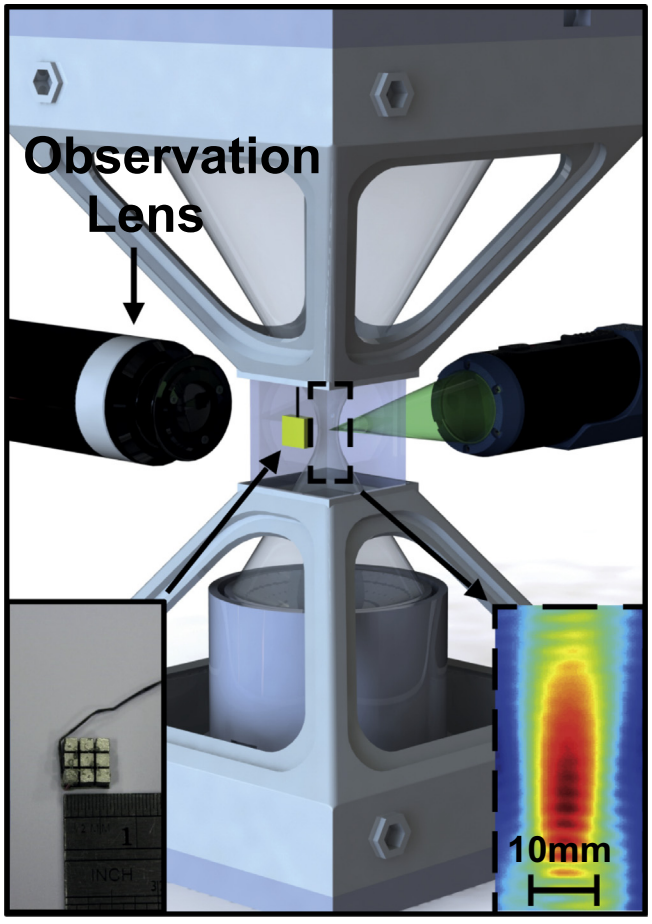

Fig. 1. Schematic representation of the sonoptic chamber, containing an upwardly propagating HIFU field from a 254 kHz source transducer, located on the base. A laser pulse (represented green) is focused through a long working distance objective lens to reproducibly nucleate single cavitation clouds in a pre-triggered HIFU burst. High-speed imaging of the activity is undertaken through an orthogonally orientated Monozoom 7 lens, opposite a liquid-light guide providing pulsed laser illumination (not shown). A passive cavitation detector (the active element of which is photographed, inset-left) is positioned next to the focus of the HIFU field, to collect acoustic data from the driven cavitation clouds. An axial scan of the HIFU focus demonstrates the field is not perturbed by the chamber (inset-right) (1.5-column).

was confirmed via comparison of pressure maps generated with a fibre-optic hydrophone (FOH, Precision Acoustics, uncalibrated at 254 kHz), through the focal zone, Fig. 1(inset-right), near- and far-fields, in both the sonoptic chamber and a free-field scanning tank ($1 \times 1 \times 1$ m^3) configuration. The focal region of the HIFU field was contained within glass walls ($32 \times 32 \times 36$ mm^3) that formed the neck of the sonoptic chamber, Fig. 1. This facilitated good optical access to that region of the field for observation, and pulsed laser irradiation to nucleate cavitation activity, as described below. Imaging was undertaken through a Monozoom 7 lens system (Bausch & Lomb, Rochester, NY, USA) set to 3.5× magnification, with a Kirana-05 M high-speed camera (Specialised Imaging, Tring, UK), recording 180 frames (924×768 pixels) at 1×10^6 frames per second (Mfps). Illumination was delivered via synchronous 20 ns laser pulses (SI-LUX 640, Specialised Imaging), coupled to a liquid light guide and a collimating lens. The camera shutter-time was set to 200 ns via its control software, although the 20 ns illumination laser pulse duration provided the effective exposure time for the images. The rate of image formation was thus 1 Mfps, but the temporal resolution for each image was 20 ns. The spatial resolution was experimentally determined as 12.3 ± 0.2 μm pixel^{-1}, via the in-situ imaging of 400 μm polymer microspheres (standard deviation 1%, Duke Standards, Fisher Scientific, Loughborough, UK). Crucially, this observation configuration conferred a degree shadowgraphic imaging, such that pressure fluctuations were visualised on account of localised refractive index variations within the host medium.

Acoustic cavitation was nucleated via a 6–8 ns 532 nm laser pulse (Nano S 130-10 frequency-doubled Q-switched Nd:YAG, Litron Lasers, Rugby, UK) of energy 0.9 ± 0.1 mJ respectively (instrument error, according to manufacturer), passed through a long working distance objective lens (50×0.42 NA Mitutoyo, Kawasaki, Japan), incident to the focal region of a pre-established HIFU field [24,25]. This pulse energy was below the optical breakdown threshold for the host medium of de-ionised water, degassed to a dissolved O_2 content below 4 mg L^{-1}, which avoided the formation of the large vapour cavity, generally associated with pulsed-laser based cavitation studies [26,27]. A total of 54 acoustic cycles were generated at the PA_{pp} of interest for a given experiment, with the nucleating-laser pulse incident ~20 μs after HIFU had propagated to the cavitation chamber. High-speed camera operation was triggered to capture 5 frames (5 μs) prior to nucleation, such that cloud development was observed from inception, and to ensure no pre-existing cavitation activity had occurred.

2.3. The passive cavitation detector and acoustic signal processing

The passive cavitation detector (PCD) used to detect the acoustic emissions presented below, was constructed from piezoceramic composite of dimensions $6 \times 6 \times 2$ mm^3, Fig. 1 (inset-left). The active element was diced to form nine distinct pillars, each ~1.5 mm^2, thereby reducing lateral mode vibrations. Silver epoxy provided the acoustic matching and acted as an electrode to the element. The device was wrapped with copper tape to provide ground and shielding, particularly from the Q-switch of the nucleating pulsed laser. A second electrode was provided via a micro-coaxial cable soldered to the element, which was isolated from the shielding.

The sensitivity of the device was previously assessed [25], via the recording of an established cavitation field, driven at very high power by a 1.17 MHz HIFU transducer (ExAblate 2000, InSightec Ltd.), under the assumption of broadband noise from inertial activity. The approach indicated a flat sensitivity centred around 500 kHz, over a bandwidth of ±350 kHz, to −6 dB.

During an experiment, the PCD was mounted on the inside of one of the glass walls, which contained the HIFU focus, within the sonoptic chamber, Fig. 1. In this position, the front face of the detector was 10–11 mm from the nucleation-laser focus, where cavitation activity was generated. Acoustic data was collected with an oscilloscope (MS07104A, Agilent Technologies) at a rate of 4 GSs^{-1} and transferred to a PC for subsequent analysis. This included low- and high-pass filtering (4th order Butterworth) at 48 and 150 kHz in MATLAB, to remove the lateral mode and fundamental driving frequencies (at 36 and 254 kHz), respectively. Fast fourier transform (FFT) operation was also used to reveal spectral features within the acoustic signal collected from the cavitation activity.

2.4. Statistical analysis

High-speed imaging observations were compared to the filtered acoustic emissions collected by the PCD, via a two tailed Pearson product-moment correlation coefficient, to determine the significance of the correlation of shock-wave detection through each modality, for each experiment. A two tailed test was chosen to assess for the possibility of a positive and negative correlation relationship. A p-value <0.01 was taken as highly significant, and <0.05 as significant.

3. Results

3.1. High-speed imaging of cavitation clouds at varying HIFU intensity

A series of preliminary experiments were initially undertaken, across the range of PA_{pp}'s available with the HIFU configuration described, at 0.1 V signal amplitude increments, limited by the maximum permissible input to the power amplifier of 1.0 V. This served to identify the key PA_{pp} values, reported below, that generated temporally stable periodic shock-wave formation from the acoustically driven clouds. At least six data sets (high-speed observation of single cavitation cloud nucleation and development, and parallel acoustic detection with the PCD) were used for analysis purposes, and the shock-wave periodicity results are reported as average value ± standard deviation.

Fig. 2 depicts sample high-speed images, extracted from sequences recorded at 1 Mfps (full sequence movies, at full field of view, available as supplementary content), of cavitation clouds evolving under HIFU of PA_{pp} (a) 0.48 ± 0.08 MPa, (b) 0.64 ± 0.12 MPa, (c) 0.92 ± 0.17 MPa and (d) 1.22 ± 0.22 MPa (RFB instrument error, according to manufacturer). Cavitation nucleation at laser incidence was taken as $t = 0$ μs. Larger clouds developed at higher intensities, due to more energetically driven fragmentation events spawning an increased number of daughter bubbles [28]. Clouds were observed to undergo collective oscillatory behaviour as we, and others, have previously reported [25,29]. Periods of inflation, during which the cloud oscillated through a series of partial contractions, are interspersed with strong collapses, from which the cloud re-inflated to enter the next oscillation stage. We refer to this repeated behaviour as being comprised of repeated growth, oscillation and collapse (GOC) cycles.

The shadowgraphic imaging facilitated the observation of periodic shock-wave generation, coincident with the cloud collapse of each GOC cycle, arrowed at $t = 106$, 114 and 122 μs in Fig. 2(a). The images of Fig. 2(c–d) were selected for equivalent collapse, and shock-emission (also arrowed), from clouds driven by higher HIFU PA_{pp}'s, at similar stages of cloud development, circa 100 μs following nucleation. The shock-waves arrowed at Fig. 2(b) 101 μs, (c) 114 μs and (d) 121 μs were the first observed from each of the clouds subsequent to those emitted at (b) 89 μs, (c), 98 μs and (d) 101 μs. The time interval between the shock-emissions is representative of the shock-period throughout the image sequence

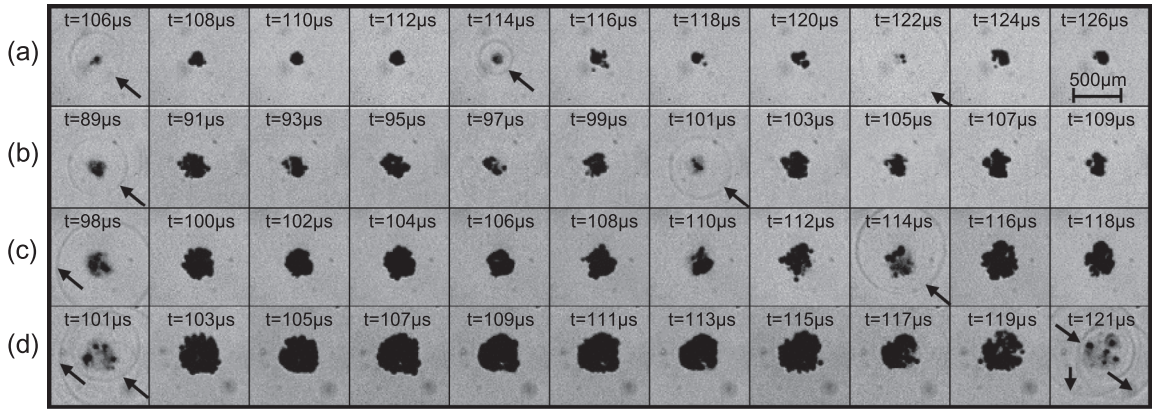

Fig. 2. Representative high-speed images extracted from sequences recorded at 1 Mfps, of cavitation cloud development under HIFU exposures of PA_{pp} (a) 0.48 MPa, (b) 0.64 MPa, (c) 0.92 MPa, and (d) 1.22 MPa. Increasing the insonation intensity increased the size of the cloud that develops, and the period of recurring shock-wave emission (arrowed black throughout), coincident to strong cloud collapse. Scale bar top-right (2-column).

acquired, which is particularly evident in the movie representation (available as supplementary content), at each PA_{pp} investigated.

These observations, recorded at 1 Mfps, only permitted an average value of ~1500 ms^{-1} to be estimated for the shock-wave propagation, consistent with the speed of sound in water at room temperature. This value of propagation speed was used to infer the moment of shock-emission used for the correlation to the acoustic data, Section 3.3.

A 7.9 ± 0.5 μs (average value over $n \geqslant 6$ data sets ± standard deviation) period of shock-wave emission from single clouds driven by PA_{pp} = 0.48 MPa, represented Fig. 2(a), corresponds to an emission frequency, f_{sw} = 127 ± 8 kHz ≈ $f_0/2$, half-harmonic to the

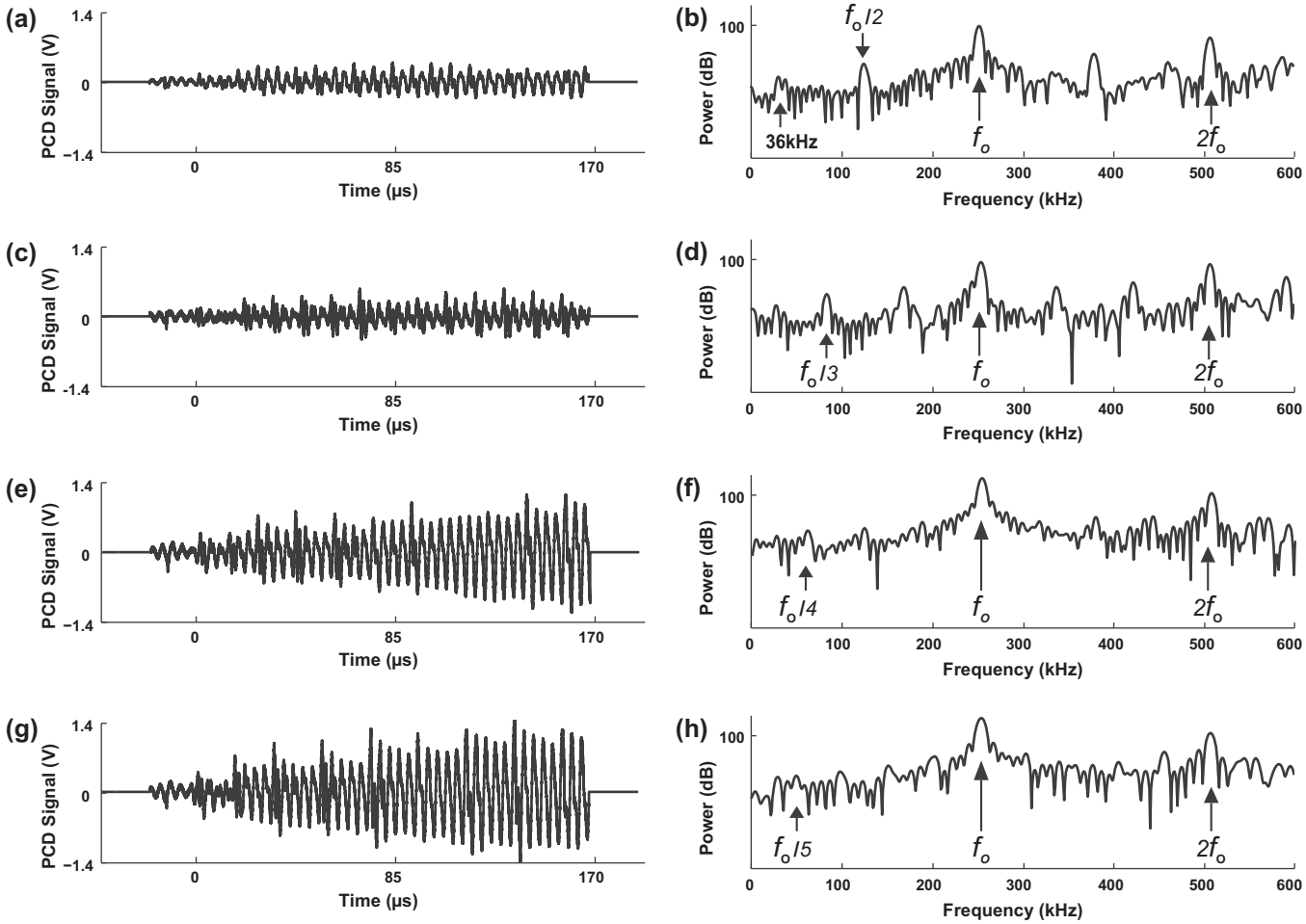

Fig. 3. (a, c, e and g) The raw acoustic signals collected by the PCD, from each of the clouds of Fig. 2, and the corresponding power spectra (b, d, f and h). The spectra are dominated by the fundamental driving at 254 kHz, and its 2nd harmonic. Also apparent are the subharmonics nf_0/m, dependent on the PA_{pp} of the driving, as well as ultra-subharmonics between f_0 and $2f_0$. The lateral mode of the transducer at 36 kHz, common to all the spectra, is noted in (b) (2-column).

driving frequency of the HIFU insonation. At 0.64 MPa, the cloud of Fig. 2(b) underwent two partial contractions, captured at t = 93 and 97 μs, during the oscillation phase of the GOC cycle, with strong collapse and coincident shock-wave emission not observed until 101 μs. An 11.8 ± 0.3 μs shock-wave period at this driving amplitude corresponds to f_{sw} = 84.6 ± 1.7 kHz ≈ $f_0/3$, the first higher-order subharmonic. Increasing the PA_{pp} of the primary insonation further, increased the period of the shock-wave emission, such that f_{sw} = 63.3 ± 1.3 kHz ≈ $f_0/4$ and 50.5 ± 0.5 kHz ≈ $f_0/5$, at 0.92 and 1.22 MPa respectively.

3.2. Extraction of the acoustic subharmonic signal

The raw acoustic data collected by the PCD, from the clouds at each HIFU PA_{pp} represented in Fig. 2, truncated to the duration of cloud observation are shown in Fig. 3(a, c, e and h), along with the corresponding power spectra from 0 to 600 kHz, Fig. 3(b, d, f and h), obtained via FFT. The fundamental driving is arrowed throughout, and the lateral mode of the HIFU transducer noted in Fig. 3(b). From all spectra collected to the data set, 126.7 ± 1.2 kHz (average value from $n \geqslant 6$ ± standard deviation), corresponds to the acoustic $f_0/2$ subharmonic for PA_{pp} = 0.48 MPa. At the higher PA_{pp}'s, spectral features at 83.8 ± 1.8, 62.8 ± 1.0 and 52.0 ± 1.6 kHz represent the higher-order subharmonics at $f_0/3$, $f_0/4$ and $f_0/5$, at driving amplitudes of 0.64, 0.92 and 1.22 MPa, respectively. The ultra-subharmonics at frequencies $>f_0$ were also apparent, Fig. 3.

In order to identify the specific acoustic signal responsible for the subharmonic features of the power spectra, the raw signals were subjected to a filtering protocol in MATLAB. This process is illustrated by Fig. 4, using the acoustic emissions from the cloud driven at PA_{pp} = 0.92 MPa, Fig. 3(e). Applying a 4th order low-pass Butterworth filter at 220 kHz produced the trace depicted in Fig. 4(a), which removed all signal > f_0, but left a significant component of the fundamental, and the subharmonics, Fig. 4(b). Further filtering with a high-pass 4th order Butterworth at 48 kHz, removed the lateral mode, and a second low-pass filter at 150 kHz removed sufficient fundamental to reveal the signal responsible for subharmonic peaks, Fig. 4(c and d), as well as residual fundamental. Finally, to verify that the filtering procedure described delivered the signal responsible for the subharmonic, Fig. 4(c) was subtracted from (a), to produce (e). The FFT of that signal, Fig 4(f), is effectively monochromatic at the fundamental, and thereby confirmed that the subharmonics had been removed. Similar treatment for the PCD data collected from the clouds at the other HIFU PA_{pp}'s, equivalently identified the acoustic data responsible for the respective subharmonics of Fig. 3(b, d and h).

3.3. Comparison of high-speed imaging and acoustic data

For direct comparison of the filtered acoustic data to the observed cloud dynamics at each HIFU PA_{pp}, we implemented a dark-pixel counting algorithm [25] to each of the high-speed image sequences, in full, represented in Fig. 2. The algorithm sums the dark-pixel number from each image sequentially, and outputs the variation with time over the observation duration, which can be taken to represent the cloud dynamics for a given experiment, Fig. 5 (grey dash lines). Through this approach, it is evident that the clouds take 20–30 μs to become established and enter stable periodic GOC cycle behaviour, which is corroborated by the movie representation of the high-speed imaging (available as supplementary content). Progressively longer GOC periods, for the larger clouds at higher intensities, are also evident through this representation.

The specific cloud collapses that produced the shock-waves highlighted in Fig. 2, are similarly arrowed in Fig. 5, along with the corresponding features within the filtered acoustic data. For convenience, we have shifted the PCD trace by −7 μs to compensate for the shock-propagation time to the detector surface. The number of collapses and shock-waves imaged via high-speed

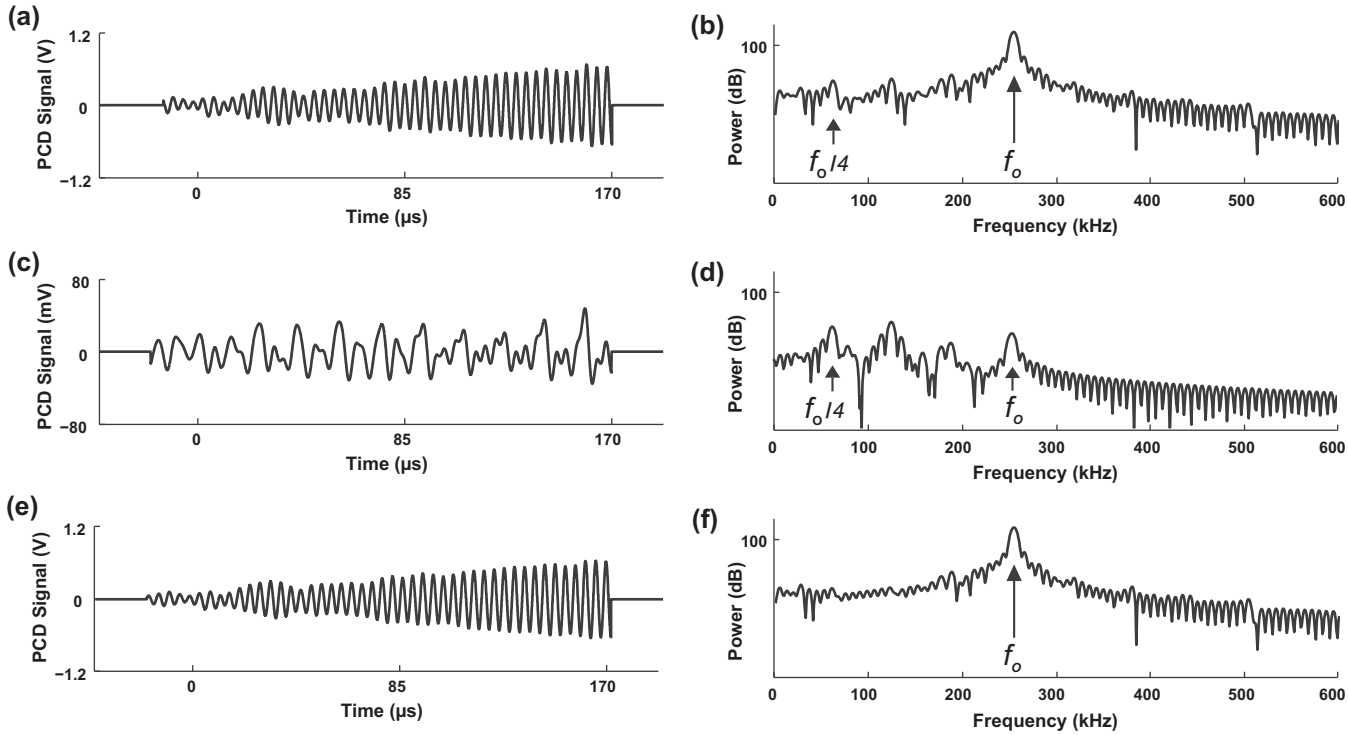

Fig. 4. (a) The acoustic data of Fig. 3(e), filtered at 220 kHz. (b) The power spectrum of (a) revealed reduced fundamental and the $nf_0/4$ subharmonics. (c) The application of a second filter at 150 kHz, removed most of the fundamental, exposing the signal responsible for the subharmonics, which were then prominent in the spectrum (d). Subtraction of signal (c) from signal (a) yielded (e), the spectrum for which (h), demonstrated the removal of the subharmonic peaks (2-column).

photography (full image sequence movies available as supplementary content) match the number of shock-waves detected by the PCD, for each PA_{pp} investigated. It is clear that the local minima of the dark-pixel curves, indicating the cloud collapse at the end of a GOC cycle, coincide with the peaks of the filtered PCD traces. Statistical analysis indicated that for $f_0/2$, there was a highly significant positive correlation between the shocks observed via high-speed photography and those detected by the PCD (p(two tailed) < 0.01), (r = 0.729, n = 17). Analysis of $f_0/3$, $f_0/4$ and $f_0/5$ data showed significant positive correlations between the two modalities (p(two tailed) < 0.05 for all three cases), (r = 0.790, n = 8) and (r = 0.816, n = 8) and (r = 0.887, n = 5), respectively.

3.4. Multiple front shock-emission from larger clouds

In contrast to the smaller clouds at lower HIFU PA_{pp}, which collapsed to give well defined, radially symmetric single-front periodic shock-waves, Fig. 2(a and b), the larger clouds at higher intensity insonations emitted multiple shock-fronts during collapse, Fig. 2(d) at t = 101 and 121 μs. This observation suggests that, for larger clouds in this experimental configuration, collapses occurred within spatially separated sub-clusters, which each independently emitted a single shock-front. Assuming radial propagation for each front, the origin of the shock-wave may be pinpointed, simply as the centre of the circle described by the component front. Moreover, the collapse time of the sub-cluster can be precisely resolved, if the propagation speed is well characterised. An illustrative example of this latter point is provided in Fig. 6, which depict three sequential frames extracted from the sequence at PA_{pp} = 1.22 MPa, 41 μs after laser-nucleation (and later represented by Fig 2(d)). The dark shadow encroaching from the bottom of these images was the ensuing negative-pressure phase of the incident HIFU, visualised through the shadowgraphy described previously and apparent for this field of view. The extended focal region of the HIFU field, Fig. 1(inset-right), led to poor optical focusing of the driving pressure fluctuations, however a propagation speed of ~1500 ms^{-1} is evident. This effect is also apparent in the movie representation of the high-speed sequences (available as supplementary content).

At this stage of the cloud development, a relatively simple structure of three distinct sub-clusters existed (labelled 1, 2 and 3). The image rate of 1 Mfps was insufficient to resolve the temporal order of collapse of the closely spaced sub-clusters. However, by 42 μs, shock-waves labelled SW1, SW2 and SW3, centred on sub-cluster 1, 2 and 3 respectively, were apparent. Assuming equivalent average propagation speeds for each shock, indicates that sub-cluster 1 collapsed first, followed by 2 approximately 110 ns later, with sub-cluster 3 collapsing last, some 80 ns after that. As such, dynamics that occurred on timescales much shorter than the imaging rate can be inferred.

In the context of PCD detection of the acoustic subharmonic from single cavitation clouds, the multiple front shock-waves will have had little bearing, as the time over which the multiple fronts of the shock-waves were spread (100's ns) was much smaller than the time between shock emission (10's μs), Figs. 2 and 6.

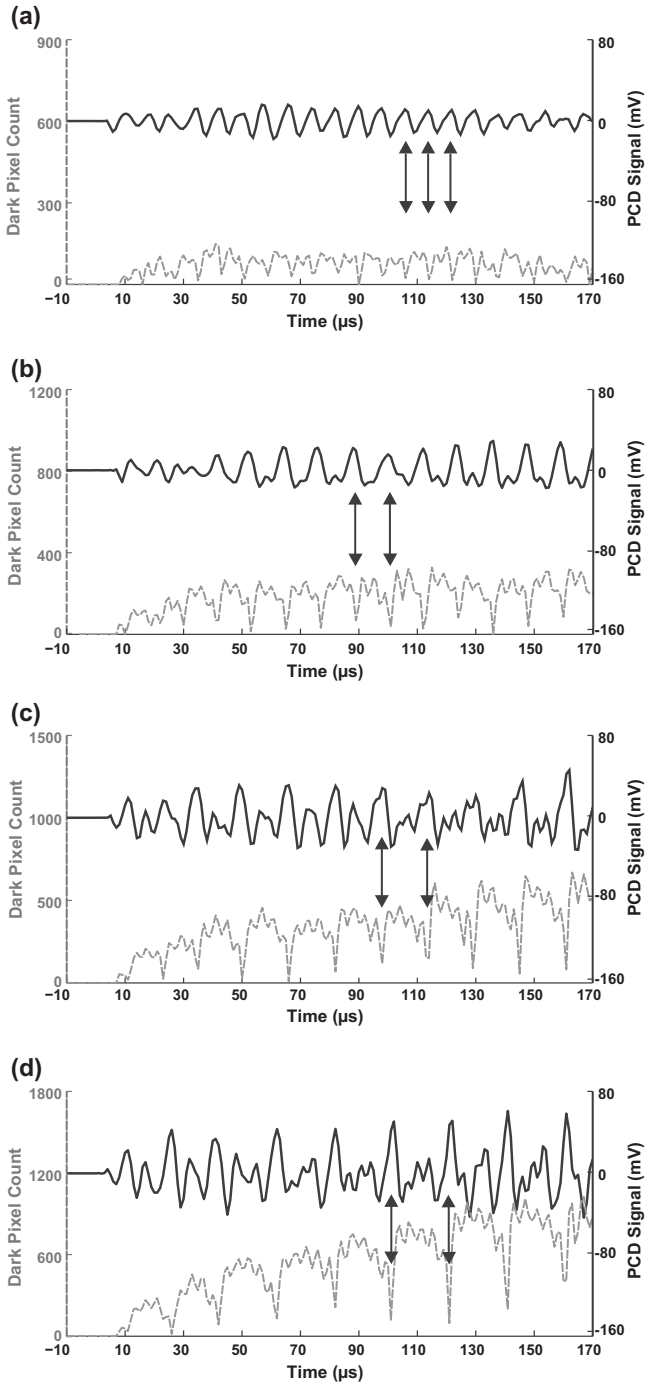

Fig. 5. (a–d) Filtered PCD data (solid) of the acoustic emissions recorded from the clouds depicted in Fig. 2(a–d, respectively). Each trace has been shifted by −7 μs to account for shock-wave propagation time to the detector. The dark pixel count (grey dashed) for the entire image sequence correlated acoustic features to the strong and periodic cloud collapses coincident with shock-emission, p(two-tailed) <0.01 (r = 0.996), over all data. (note different scales selected for ease of viewing) (1.5-column).

4. Discussion

The high-speed camera used for this work provided 180 frames at the image-acquisition rates required to resolve cavitation dynamics, driven by HIFU in the 100's of kHz regime. Moreover, sufficient PCD data can be collected over this time-scale for meaningful analysis, and direct correlation to the resolved cloud dynamics. The combination of imaging duration and temporal resolution, together with synchronous pulsed-laser illumination, facilitated the novel observation of a significant number of periodic shock-waves emitted from single clouds of cavitation bubbles over ~50 cycles of HIFU insonation, across a range of intensities. A relatively large field of view (see movie representations available as supplementary content) ensured that no shock-waves were missed during high-speed sequence acquisition, despite the 20 ns effective exposure time, per frame, provided by the pulsed laser illumination.

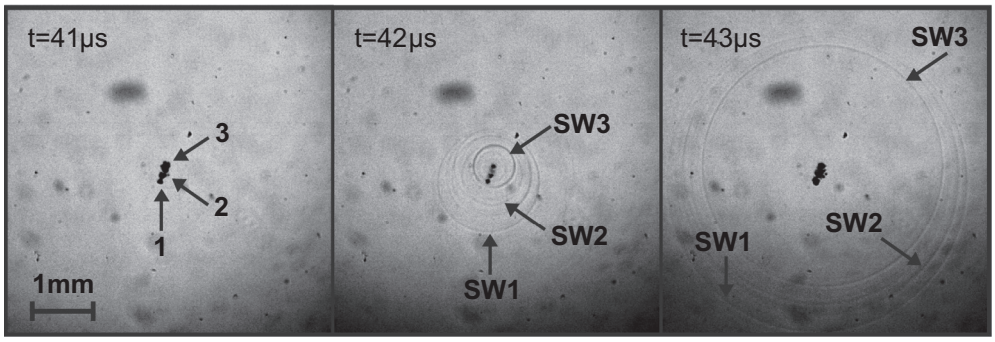

Fig. 6. Earlier frames from the high-speed sequence recorded at HIFU PA_{pp} = 1.22 MPa. At 42 μs, three shock-waves (SW1-3) have emerged, each centred on a sub-cluster (1-3, at 41 μs). The distance propagated by each shock, relative to the others at any given instant, is indicative of the temporal order of collapse for the source sub-clusters. Scale bar bottom-left (1.5-column).

Systematically increasing the intensity of the HIFU increased the period of shock-wave emission, in accordance with the growth, oscillation and collapse cycles observed for the clouds. The most significant finding of this research is that the shock-wave emission occurred at frequencies subharmonic to the driving, and at higher orders for higher intensity insonations, up to $f_0/5$. At HIFU PA_{pp} values intermediate to those reported, stable periodic shock-wave emission was not observed. This was either manifested as a switching between the shock-periods of the stable emission PA_{pp} values above and below the intermediate value, or a failure to undergo the strong collapses required to generate observable shock-waves. In both cases, the associated acoustic data was ambivalent, with no clear spectral features apparent.

Reconciling the acoustic profiles of the shock-waves to the repetitive collapses of the observed cavitation clouds and the power spectra of the PCD signals, Fig. 5, confirmed that periodic shock-emission provides a previously unidentified source for the cavitation subharmonic signal. Subtraction of the acoustic profile of the shock-waves from the overall PCD recording of the cloud emissions, and consequent purging of the subharmonic peaks from the spectra, Fig. 4(f), demonstrated conclusively the role of the periodic shock-waves. The shock-wave nature underpinning this mechanism of subharmonic signal generation, has particular significance in terms of the optimisation of detection devices. It is worth noting that individual shock-waves are inherently broadband in the frequency domain [9,10]. Indeed, the PCD used for this work has poor sensitivity at frequencies <100 kHz. We therefore hypothesise that subharmonic-detection was achieved principally via the higher-frequency content of the individual shocks, and that the spectral features arise from the periodicity of shock-emission.

The generation of a single shock-wave from a transient HIFU-generated hemispherical cavitation cloud, collapsing under static ambient pressure in proximity to a surface, has been observed before [30]. This study used high-speed imaging at 200 Mfps, over a shorter observation duration, and reported an initial shock-wave propagation speed of ~2600 ms^{-1}. However, they also noted rapid deceleration of the shock within 20 ns of emission, to a velocity of 1500 ms^{-1} as observed in this study. Moreover, the critical role of cloud collapse in applications such as material erosion has been demonstrated [31]. In the current report, the link between periodic collapse from a continuously driven cloud, coincident shock-emission, and the cavitation subharmonic signal is established, potentially consolidating a growing volume of literature that links cavitation related effects to the onset of the subharmonics specifically [1–7], across a range of applications. This suggests that cloud dynamics, arising from a number of mutually interacting component bubbles in close proximity, could be a key factor to cavitation-mediated effects, rather than the activity of single bubbles responding to an insonation individually.

The period-doubled, half-harmonic response of the cloud at lower intensity HIFU driving at f_0, and the successive higher-order subharmonic cycles on increasing the intensity, indicates that the cloud system progresses through several regimes of non-linearity [10,25]. Further work is certainly required to theoretically describe this response in terms of a bubble-ensemble responding to continuous acoustic driving. Understanding intra-cloud collapse dynamics at the component bubble scale is, however, a significant challenge, particularly for densely packed clouds of a large number of component bubbles, such as those observed here. One model of cloud collapse, proposed by Hansson and Mørch [32] in an attempt to explain material erosion effects, considered the collapse of cylindrical and hemispherical clouds of bubbles in the vicinity of surfaces, driven by an ultrasonic horn operating at 20 kHz. It was suggested that a series of inwardly collapsing shells, with the energy from the collapse of one shell amplifying the collapse of the next, was a plausible mechanism for reaching the conditions required to yield the observed erosion. The observations of multiple-front shock-waves of Figs. 2(d) and 6 indicate that sub-clusters within a cloud under higher driving pressure amplitudes, and far from any surfaces, indeed collapse at different times and at distinct locations within the cloud, but do not seem to conform to the sequential shell-model. We propose that multiple front shock-wave observation may provide a tool with which intra-cloud collapse may be probed for high void fraction systems, and at nanosecond temporal resolution.

Further work will also seek to identify the transition to inertial cavitation, with the associated marked increase in broadband signal [9,10], which remains an outstanding issue. It is conceivable that a medium hosting a significant number of clouds, each undergoing incoherent GOC cycles could generate shock-waves with no discernible periodicity, that may therefore appear broadband to an acoustic detector. Moreover, the observation of multiple front shock-waves from larger clouds collapsing non-uniformly, could have a contributory frequency-broadening effect. Indeed, the generation of other acoustic signals may be expected, for example from the partial deflations the clouds undergo during the oscillation phase of the GOC cycle, but at pressure amplitudes below the threshold for visualisation via refractive index modulation for the shadowgraphic imaging configuration used here.

5. Conclusion

We present conclusive experimental evidence for a source of the cavitation subharmonic (and higher-order subharmonics) acoustic signal, that applies to strongly driven bubble cloud systems. Via high-speed shadowgraphic imaging, clouds are observed to undergo growth, oscillation and collapse cycles, periodically

emitting shock-waves coincident to the moment of collapse. We have thus demonstrated that for oscillating cloud systems the subharmonic is a discretely, rather than continuously, emitted signal. The GOC cycles, frequency of shock-wave emission, and therefore order of the subharmonic detected, are primarily determined by the intensity of the insonation.

Acknowledgements

The research leading to these results has received funding from the European Research Council under the European Union's Seventh Framework Programme (FP/2007-2013)/ERC Grant Agreement no. 336189 (TheraCav). K.J., C. T.-S. and A.C. acknowledge support through the ERC FP7 Grant CoDIR. B.G. received support from the Scottish Universities Physics Alliance (SUPA), via the Industrial Placement scheme. The Norwegian authors are also grateful to the Michelsen Centre of Industrial Measurement and Instrumentation, Bergen, Norway.

Appendix A. Supplementary material

Supplementary data associated with this article can be found, in the online version, at http://dx.doi.org/10.1016/j.ultras.2014.06.011.

References

[1] Y. Son, M. Lim, J. Khim, M. Ashokkumar, Acoustic emission spectra and sonochemical activity in a 36 kHz sonoreactor, Ultrason. Sonochem. 19 (1) (2012) 16.
[2] C. Koch, K.V. Jenderka, Measurement of sound field in cavitating media by an optical fibre-tip hydrophone, Ultrason. Sonochem. 15 (4) (2008) 502.
[3] S.D. Sokka, R. King, K. Hynynen, MRI-guided gas bubble enhanced ultrasound heating in in vivo rabbit thigh, Phys. Med. Biol. 48 (2) (2003) 223.
[4] K.I. Morton, G.R. ter Haar, I.J. Stratford, C.R. Hill, Subharmonic emission as an indicator of ultrasonically-induced biological damage, Ultrasound Med. Biol. 9 (6) (1983) 629.
[5] N.I. Vykhodtseva, K. Hynynen, C. Damianou, Histologic effects of high-intensity pulsed ultrasound with subharmonic emission in rabbit brain in vivo, Ultrasound Med. Biol. 21 (7) (1995) 969.
[6] G.A. Husseini, M.A.D. de la Rosa, E.S. Richardson, D.A. Christensen, W.G. Pitt, The role of cavitation in acoustically activated drug delivery, J. Control. Release 107 (2) (2005) 253.
[7] C. Coussios, C.H. Farny, G.R. ter Haar, R. Roy, Role of acoustic cavitation in the treatment and monitoring of cancer treatment by high-intensity focused ultrasound, Int. J. Hyperthermia 23 (92) (2007) 105.
[8] E.A. Neppiras, Acoustic cavitation, Rep. Phys. 61 (3) (1980) 159.
[9] T.G. Leigthon, The Acoustic Bubble, Academic Press, London, 1994.
[10] W. Lauterborn, T. Kurz, Physics of bubble oscillations, Rep. Prog. Phys. 73 (10) (2010) 106501.
[11] W. Lauterborn, E. Cramer, Sub-harmonic route to chaos observed in acoustics, Phys. Rev. Lett. 47 (20) (1981) 1445.
[12] X.M. Yang, R.A. Roy, R.G. Holt, Bubble dynamics and size distribution during focused ultrasound, J. Acoust. Soc. Am. 116 (6) (2004) 3431.
[13] M. Postema, P. Marmottant, C.T. Lancée, S. Hilgenfeldt, N. De Jong, Ultrasound-induced microbubble coalescence, Ultrasound Med. Biol. 30 (10) (2004) 1337.
[14] J.T. Tervo, R. Mettin, W. Lauterborn, Bubble cluster dynamics in acoustic cavitation, Acta Acoust. 92 (1) (2006) 178.
[15] E.A. Neppiras, Subharmonic and other low-frequency emission from sound-irradiated liquids, J. Acoust. Soc. Am. 46 (3P2) (1969) 587.
[16] S. Khanna, N.N. Amso, S.J. Paynter, W.T. Coakley, Contrast agent bubble and erythrocyte behaviour in a 1.5 MHz standing ultrasound field, Ultrasound Med. Biol. 29 (10) (2003) 1463.
[17] J. Silj, B. Dollet, M. Overvelde, V. Garbin, T. Rozendal, N. de Jong, D. Lohse, M. Versluis, Subharmonic behaviour of phospholipid-coated ultrasound contrast agent microbubbles, J. Acoust. Soc. Am. 128 (5) (2010) 3239.
[18] M.S. Longuet-Higgins, Monopole emission of sound by asymmetric bubble oscillations.1. Normal modes, J. Fluid Mech. 201 (1989) 525.
[19] A. Eller, H.G. Flynn, Generation of subharmonics of order one-half by bubbles in a sound field, J. Acoust. Soc. Am. 46 (3P2) (1969) 722.
[20] A. Prosperetti, Nonlinear oscillations of gas-bubbles in liquids – transient solutions and connection between subharmonic signal and cavitation, J. Acoust. Soc. Am. 57 (4) (1975) 810.
[21] A. Prosperetti, A general derivation of the subharmonic threshold of non-linear bubble oscillations, J. Acoust. Soc. Am. 133 (6) (2013) 3719.
[22] A.F. Prokop, A. Soltani, R.A. Roy, Cavitational mechanisms in ultrasound-accelerated fibrinolysis, Ultrasound Med. Biol. 33 (6) (2007) 924.
[23] T.G. Muir, E.L. Carstensen, Prediction of non-linear acoustic effects at biomedical frequencies and intensities, Ultrasound Med. Biol. 6 (4) (1980) 345.
[24] B. Gerold, S. Kotopoulis, C. McDougall, D. McGloin, M. Postema, P. Prentice, Laser-nucleated acoustic cavitation in focused ultrasound, Rev. Sci. Inst. 82 (4) (2011) 044902.
[25] B. Gerold, I. Rachmilevitch, P. Prentice, Bifurcation of ensemble oscillations and acoustic emissions from early stage cavitation clouds in focused ultrasound, New J. Phys. 15 (2013) 033044.
[26] A. Vogel, S. Busch, U. Parlitz, Shock wave emission and cavitation bubble generation by picosecond and nanosecond optical breakdown in water, J. Acoust. Soc. Am. 100 (1) (1996) 148.
[27] B. Gerold, P. Glynne-Jones, C. McDougall, D. McGloin, S. Cochran, A. Melzer, P. Prentice, Directed jetting from collapsing cavities exposed to focused ultrasound, Appl. Phys. Lett. 100 (2) (2012) 024104.
[28] M. Postema, A. Van Wamel, C.T. Lancée, N. De Jong, Ultrasound-induced encapsulated microbubble phenomena, Ultrasound Med. Biol. 30 (6) (2004) 827.
[29] Y. Lu, J. Katz, A. Prosperetti, Dynamics of cavitation clouds within a high-intensity focused ultrasonic beam, Phys. Fluids 25 (7) (2013) 073301.
[30] E.A. Brujan, T. Ikeda, Y. Matsumoto, Shock wave emission from a cloud of bubbles, Soft Matter 8 (21) (2012) 5777.
[31] B.R. Birkin, D.G. Offin, C.J.B. Vian, T.G. Leighton, Multiple observations of cavitation cluster dynamics close to an ultrasonic horn tip, J. Acoust. Soc. Am. 130 (5) (2011) 3379.
[32] I. Hansson, K.A. Mørch, The dynamics of cavity clusters in ultrasonic (vibratory) cavitation erosion, J. Appl. Phys. 51 (9) (1980) 4651.